ChemComm

COMMUNICATION

View Article Online
View Journal | View Issue

Cite this: *Chem. Commun.*, 2024, **60**, 2365

Received 22nd November 2023,
Accepted 29th January 2024

DOI: 10.1039/d3cc05725a

rsc.li/chemcomm

Insights into interfacial mechanisms: $CsPbBr_3$ nanocrystals as sustainable photocatalysts for primary amine oxidation†

Monika Ahlawat and Vishal Govind Rao *

$CsPbBr_3$ nanocrystals (NCs) employed as a photocatalyst resulted in efficient benzylamine oxidation under oxygen atmosphere. Improved reaction yields stem from favorable $-NH_2$ functional group interactions on the NC surface, while additional interactions with −OMe or −SMe functional groups post-product formation result in lower yields. These insights into interfacial interactions and mechanistic aspects advance sustainable chemical transformations through cost-effective and recyclable $CsPbBr_3$ NC-catalyzed primary amine oxidation.

The long charge carrier diffusion lengths and low surface trap densities of lead halide perovskites (LHPs) have underpinned their success in photovoltaics with photoconversion efficiencies exceeding 25%.[1,2] Recent studies have unveiled their potential as photocatalysts in reactions such as water splitting, CO_2 reduction, dye degradation, polymerization, and organic synthesis.[3–12] However, LHPs face challenges due to their structural instability in polar solvents. To address this, various strategies, including ligand engineering, surface encapsulation, and heterojunction formation, have been explored.[8,13–15] Their band gap tunability through halide exchange offers opportunities for tailoring their selectivity in organic reactions.[3] While inorganic LHPs, primarily $CsPbBr_3$, have been favored for organic transformations due to their suitable band gap and robust chemical stability under reaction conditions, the potential of surface interactions between these perovskites and reactant molecules remains untapped.[3,16–22] Exploring these interactions offers a pathway to unveil mechanistic insights, enhance reaction yields, and fine-tune selectivity. Primary amines, as reactants, are particularly intriguing due to their specific interactions with perovskite surfaces.[23] Moreover, the formation of imines using perovskite photocatalysts has received limited attention thus far. Therefore, the direct oxidative coupling of amines to imines under mild conditions, without additional reagents, presents an enticing and underexplored area with considerable potential for applications in pharmaceuticals and sustainable chemical synthesis.[24–26]

In this study, we explored the role of interfacial interactions between a reactant (benzylamine and its derivatives) and the $CsPbBr_3$ nanocrystal (NC) surface in directing the reaction yield of photocatalytic oxidation of primary amines to imines under optimized conditions and utilizing O_2 as an oxidant. Due to their prevailing electronic effects, the strong interactions with –OMe and –SMe groups (along with the NH_2 group) present in 4-methoxy and 4-(methylthio)-substituted benzylamines possibly hinder the detachment of the molecule from the surface after product formation, diminishing the overall yield as compared to the standard benzylamine. Mechanistic investigations revealed a radical pathway, generating *N*-radical cations and superoxide radical anions (from O_2) by capturing photogenerated holes and electrons, respectively, from $CsPbBr_3$ NCs. Furthermore, the $CsPbBr_3$ NCs exhibit stability under standard reaction conditions and can be reused for up to four cycles with a satisfactory yield. This study underscores the potential of $CsPbBr_3$ NCs in selective photocatalysis for organic synthesis, with a particular focus on primary amines due to their specific interactions with perovskite surfaces.

$CsPbBr_3$ NCs were synthesized using the hot-injection method, following established protocols.[27] Subsequently, we assessed their structural and optical properties as discussed in ESI,† Fig. S1. The $CsPbBr_3$ NCs were employed to catalyze the synthetic transformation of benzylamine to *N*-benzylidenebenzylamine in toluene under visible light irradiation at room temperature (experimental details present in ESI† Section S6). We conducted a comprehensive analysis of the reaction intermediates and products using ^1H nuclear magnetic resonance (NMR), ^{13}C NMR, and gas-chromatography-mass spectrometry (GC-MS). The reaction conditions were optimized to achieve a yield of approximately 73% after 10 hours of exposure to light and under constant O_2 pressure (as detailed in Sections S6 and S8, ESI†). In all photocatalytic reactions, the yield was

Department of Chemistry, Indian Institute of Technology Kanpur, Kanpur, 208016, Uttar Pradesh, India. E-mail: vgrao@iitk.ac.in

† Electronic supplementary information (ESI) available. See DOI: https://doi.org/10.1039/d3cc05725a

Table 1 Standard photocatalytic reaction scheme and control experiments

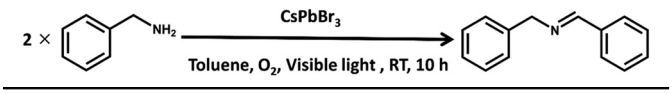

Entry	Reaction conditions	Percent yield
1	Standard	73
2	Without O_2 (N_2 balloon)	31
3	Without light	2
4	Without $CsPbBr_3$ NCs	4
5	With hole scavenger (ethanol)	11
6	With $O_2^{\bullet-}$ radical scavenger (Proline)	15

Reaction conditions: $CsPbBr_3$ NCs (6 mM, 0.4 mL), benzylamine (1 M, 60 μl), light (450 mW cm^{-2}), time (10 h), O_2 atmosphere.

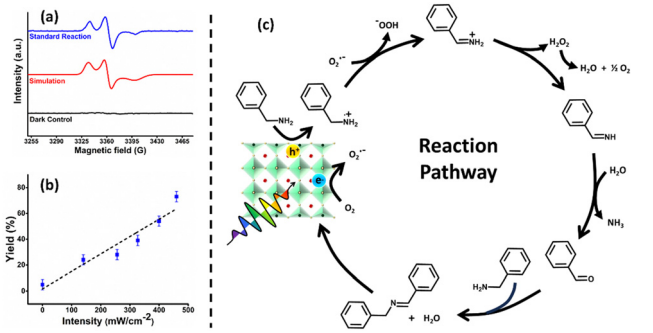

Fig. 1 Mechanistic pathway of the oxidative reaction. (a) EPR spectrum obtained for the standard reaction under both light-irradiated and non-irradiated conditions, utilizing DMPO as a spin-trapping agent. (b) The linear dependence of reaction yield on light intensity, illustrating the involvement of photogenerated charge carriers in the reaction pathway. (c) Schematic representation of the likely reaction pathway for the oxidative photocatalytic conversion of benzylamine into *N*-benzylidenebenzylamine.

calculated from ^{1}H NMR spectroscopic analysis where mesitylene served as the internal standard for product quantification. Notably, the sole product of the photocatalytic reaction was *N*-benzylidenebenzylamine, as depicted in Fig. S2 (ESI†), with benzaldehyde as an intermediate. Confirmation of *N*-benzylidenebenzylamine as the reaction product was further demonstrated through analysis of ^{13}C NMR spectrum (Fig. S3, ESI†) and GC-MS results (Fig. S4 and S5, ESI†) obtained from the same sample.

We investigated the potential influence of various reaction variables, including light, O_2, and $CsPbBr_3$ NCs (Table 1). Notably, in the absence of $CsPbBr_3$ NCs and under dark conditions, we observed no significant product formation (Fig. S6 and S7, respectively, ESI†). Furthermore, substituting O_2 with N_2 in the reaction mixture led to a notable decrease in reaction yield (Fig. S8, ESI†). These findings strongly indicate that the transformation of benzylamine to *N*-benzylidenebenzylamine is a photocatalytic process, with O_2 playing a pivotal role in the reaction mechanism. Drawing upon our knowledge of the electron–hole dynamics within $CsPbBr_3$ NCs and potential photocatalytic reaction pathways, we initially hypothesized a radical-mediated process. Accordingly, we performed the reaction in the presence of a hole scavenger (ethanol) and $O_2^{\bullet-}$ scavenger (proline).[28,29] A significant decrease in the reaction yield in both cases (shown in Table 1 and Fig. S9, ESI†) provided compelling evidence of the pivotal role played by photogenerated holes and electrons. The photogenerated holes would be responsible for oxidizing the benzylamine substrate, whereas the electrons were being captured by O_2 to generate $O_2^{\bullet-}$ radicals. The alignment of the oxidation and reduction potential of benzylamine and O_2, respectively, corroborates the assertion of concurrent photogenerated electron and hole transfer from the surface of the $CsPbBr_3$ NCs.[30] Furthermore, we anticipate a robust interaction between benzylamine and the $CsPbBr_3$ NCs,[31] thereby enhancing the probability of capturing photogenerated electrons and holes. This, in turn, facilitates their simultaneous extraction from the NC surface.

To further validate the radical pathway in the oxidative photocatalytic reaction, we conducted electron paramagnetic resonance (EPR) spectroscopic analysis, employing 5,5-dimethyl-1-pyrroline *N*-oxide (DMPO) as a spin-trapping agent. The results corroborated this pathway, revealing a hyperfine splitting indicative of DMPO adduct formation with both *N*-cations and $O_2^{\bullet-}$ radicals, as shown in Fig. 1a.[32] Consequently, the generation of highly unstable H_2O_2 occurs, which may undergo further decomposition into H_2O and dioxygen through imine formation.[30] This process leads to the hydrolysis of the imine product, resulting in the formation of benzaldehyde, as observed in NMR analysis. Subsequently, benzaldehyde reacts with the amine, giving rise to the final product, *N*-benzylidenebenzylamine.

Our understanding of the photocatalytic behavior of $CsPbBr_3$ NCs was further advanced by investigating the relationship between light intensity and reaction yield, which demonstrated linearity (as depicted in Fig. 1b). This observation illustrates an energetic charge carrier-driven process[33] and reinforces the established photocatalytic activity of $CsPbBr_3$ NCs in the oxidative coupling of amines for imine formation. Therefore, drawing from the results obtained in various control experiments, Fig. 1c outlines the plausible reaction pathway for the photocatalytic conversion of benzylamine into *N*-benzylidenebenzylamine.

The occurrence of the photocatalytic reaction for substituted benzylamines, such as 4-methoxybenzylamine and 4-(methylthio)-benzylamine substrates, demonstrates the potential of oxidative coupling reactions for imine formation using $CsPbBr_3$ NCs as photocatalysts (as shown in Fig. S11 and S12, ESI†). Activating groups such as –OMe and –SMe at the para position of benzylamine are known to enhance the rate of reactions involving nitrogen radicals during the oxidation of primary amines due to their electronic effects.[34,35] However, we observed significantly lower yields compared to the standard benzylamine oxidation reaction (as presented in Table S1, ESI†).

We speculated that the –OMe and –SMe substituent groups played a role in producing these lower yields. It is well-known that ligands or molecules containing N, O, and S atoms can strongly interact with the perovskite surface by passivating surface traps/vacancies or stabilizing dangling surface ions through electrostatic interactions and hydrogen bonds.[23,31]

Firstly, we assessed the photoluminescence (PL) response (excitation at 365 nm) of $CsPbBr_3$ NCs to monitor the passivation

effect of all three reactant molecules. As expected, the PL intensity of the $CsPbBr_3$ NCs (22 nM in toluene) significantly increased (approximately 42%) with the addition of benzylamine, indicating surface passivation due to the $-NH_2$ group (Fig. S13a, ESI†). Interestingly, the increase in PL intensity was even higher for 4-methoxybenzylamine (around 64%) and 4-(methylthio)benzylamine (approximately 53%), suggesting better passivation of the $CsPbBr_3$ NCs' surfaces through additional –OMe and –SMe interactions. Therefore, it is highly likely that –OMe and –SMe groups can serve as additional anchoring groups, interacting with the perovskite surface *via* O and S atoms, respectively.[23] Time-resolved PL measurements aligned with steady-state measurements, revealing a notable increase in the PL lifetime of $CsPbBr_3$ NCs in the presence of benzylamine and its para-substituted derivatives, as illustrated in Fig. S13b and Table S2 (ESI†). However, no discernible alteration in the crystal structure of $CsPbBr_3$ NCs was observed upon treatment with the amines, as depicted in Fig. S14 (ESI†). Fourier-transformed infrared and X-ray photoelectron spectroscopic analyses further confirmed the interfacial interaction between the amine reactant molecules and the surface of the $CsPbBr_3$ NCs, as depicted in Fig. S15 (ESI†).

To further investigate these interactions between reactant molecules and the $CsPbBr_3$ NC surface, we employed 2D-nuclear Overhauser effect spectroscopy (2D-NOESY), a powerful tool for studying NC-ligand binding and the dynamic interface.[13,36,37] In addition to the native ligands (oleylamine and oleic acid), we observed negative cross peaks corresponding to the amine A protons and neighboring B protons in the standard benzylamine reactant (as shown in Fig. 2a). These negative cross peaks indicated that benzylamine molecules were bound to $CsPbBr_3$ NCs and were tumbling slowly within the influence of the NCs.[37] Interestingly, the 2D NOESY spectrum of 4-methoxybenzylamine and 4-(methylthio)benzylamine in the presence of $CsPbBr_3$ NCs showed negative cross peaks not only for protons corresponding to $-NH_2$ anchoring groups but also for –OMe and –SMe protons, as depicted in Fig. 2b and c, respectively. These results suggest strong interactions of the reactant molecules *via* N atoms in all three substrates, along with O atoms in 4-methoxybenzylamine and S atoms in 4-(methylthio)benzylamine as shown in the corresponding bottom panels of Fig. 2. The strong interaction through both $-NH_2$ and –OMe/–SMe groups may enhance initial access to catalytic sites. However, the retention of product molecules on the NC surface through –OMe/–SMe interactions may subsequently lead to steric hindrance and limited access to catalytic sites for other reactant molecules. This is depicted in Scheme S1 in the ESI.† In contrast, no such interaction is possible after the formation of the product in the standard benzylamine reaction, allowing catalytic sites to remain available for other molecules and thus increasing the reaction yield.

Regarding the stability and recyclability of the catalyst, the $CsPbBr_3$ NCs were stable in the reaction conditions and could be reused for at least four cycles. The stability may be attributed to favorable interactions between the amine functionality in the

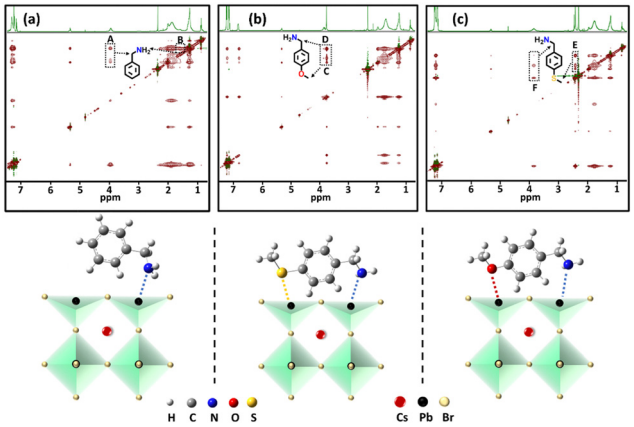

Fig. 2 2D NOESY spectrum showing (a) benzylamine, (b) 4-methoxybenzylamine and (c) 4-(methylthio)benzylamine interactions with $CsPbBr_3$ NCs in $CDCl_3$ and corresponding schematics in the bottom panel showing their plausible interaction on the NC's surface. Negative cross peaks corresponding to substrates are highlighted to show their bound nature or interaction with $CsPbBr_3$ NCs.

substrate (benzylamine) and the surface of the NCs. Such interactions likely prevented any disruption of the dynamic ligand shell of the $CsPbBr_3$ NCs, which could have occurred during the reaction. Comparative absorption and emission spectra of pure $CsPbBr_3$ NCs and the reaction mixture (Fig. 3a) acquired after completing the standard reaction showed that the excitonic features remained intact, confirming the stability of the NCs during the reaction. Photographic images of the reaction mixture before and after the reaction are presented in Fig. S16 (ESI†). After the reaction, $CsPbBr_3$ NCs were subjected to washing with acetone as an antisolvent and then characterized using transmission electron microscopy (TEM) and NMR (Fig. 3b and Fig. S17, respectively, ESI†).

The powder X-ray diffraction pattern after the reaction (Fig. S18, ESI†) further confirms the crystallographic stability of the $CsPbBr_3$ NCs. It is essential to acknowledge that there is some catalyst loss during each wash (Fig. 3c and Section S12 in the ESI†). Additionally, the perovskite structure/nanocrystals inherently exhibit sensitivity, especially in ambient conditions, and this sensitivity may further increase under the reaction conditions, such as in an excess O_2 atmosphere. Additionally,

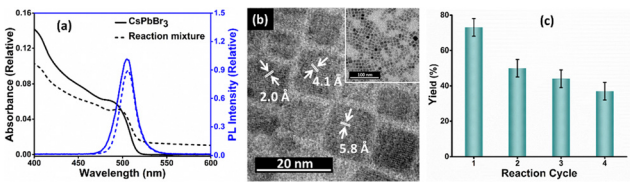

Fig. 3 Stability and recyclability of $CsPbBr_3$ NCs. (a) Comparative absorption and emission spectrum of $CsPbBr_3$ NCs and the reaction mixture after completion of the standard reaction. (b) TEM image of $CsPbBr_3$ NCs showing the retention of the size and crystallographic phase of the NCs after the first cycle of photocatalytic reaction. (c) Reaction yield obtained during each cycle of the photocatalytic reaction performed under standard reaction conditions.

the formation of H_2O as a side product might contribute to the reduction in reaction yield with each successive cycle.

In conclusion, we build upon the role of interfacial interactions between reactant/product molecules and $CsPbBr_3$ NCs determining the reaction yield by overcoming the electronic effects of substituent groups. This study establishes $CsPbBr_3$ NCs as a promising next-generation photocatalyst for the oxidative coupling of primary amines to imines. Notably, the simultaneous utilization of photogenerated holes and electrons from $CsPbBr_3$ NCs eliminates the need for scavenging agents, which were previously essential components in conventional semiconductor-based photocatalytic coupling reactions. The cost-effective and straightforward synthesis of $CsPbBr_3$ NCs holds significant potential for translational research in organic transformations, particularly in cases where complex and expensive approaches, such as noble metal-based catalysts, pose limitations as commercial photocatalysts.

V. G. R. acknowledges the Science and Engineering Research Board, Government of India, for financial support (Grant No. CRG/2022/000420). V. G. R. also acknowledges the Indian Institute of Technology Kanpur for infrastructure and initial funding to set up the lab. M. A. thanks the Indian Institute of Technology Kanpur for the research fellowship. We also thank Prof. Apparao Draksharapu for providing access to the GC-MS facility. M. A. thanks Mr Shivendra Singh for his assistance with time-resolved PL measurements.

Conflicts of interest

There are no conflicts to declare.

Notes and references

1 A. Kostopoulou, K. Brintakis, N. K. Nasikas and E. Stratakis, *Nanophotonics*, 2019, **8**, 1607–1640.
2 M. Ahlawat, S. Kumari and V. Govind Rao, *J. Mater. Chem. A*, 2023, **11**, 13289–13299.
3 K. Ren, S. Yue, C. Li, Z. Fang, K. A. M. Gasem, J. Leszczynski, S. Qu, Z. Wang and M. Fan, *J. Mater. Chem. A*, 2022, **10**, 407–429.
4 J. San Martin, N. Dang, E. Raulerson, M. C. Beard, J. Hartenberger and Y. Yan, *Angew. Chem., Int. Ed.*, 2022, **61**, e202205572.
5 I. Rosa-Pardo, D. Zhu, A. Cortés-Villena, M. Prato, L. De Trizio, L. Manna, R. E. Galian and J. Pérez-Prieto, *ACS Energy Lett.*, 2023, **8**, 2789–2798.
6 I. Rosa-Pardo, C. Casadevall, L. Schmidt, M. Claros, R. E. Galian, J. Lloret-Fillol and J. Pérez-Prieto, *Chem. Commun.*, 2020, **56**, 5026–5029.
7 K. Wang, H. Lu, X. Zhu, Y. Lin, M. C. Beard, Y. Yan and X. Chen, *ACS Energy Lett.*, 2020, **5**, 566–571.
8 S. Schünemann, M. van Gastel and H. Tüysüz, *ChemSusChem*, 2018, **11**, 2057–2061.
9 M. Ahlawat, Neelakshi, R. Ramapanicker and V. Govind Rao, *ACS Appl. Mater. Interfaces*, 2024, **16**, 623–632.
10 X. Zhu, Y. Lin, Y. Sun, M. C. Beard and Y. Yan, *J. Am. Chem. Soc.*, 2019, **141**, 733–738.
11 A. Manna, T. K. Dinda, S. Ghosh and P. Mal, *Chem. Mater.*, 2023, **35**, 628–637.
12 W. Sun, S.-Z. Zhang, Y.-J. Xue, L.-P. Mo and Z.-H. Zhang, *J. Photochem. Photobiol., A*, 2022, **432**, 114070.
13 M. Ahlawat, Neelakshi, R. Ramapanicker and V. Govind Rao, *ACS Energy Lett.*, 2023, **8**, 2159–2168.
14 A. Kipkorir, J. DuBose, J. Cho and P. V. Kamat, *Chem. Sci.*, 2021, **12**, 14815–14825.
15 P. Aggarwal, A. Halder, Neelakshi, R. Ramapanicker and V. Govind Rao, *ACS Energy Lett.*, 2023, **8**, 1520–1528.
16 J. T. DuBose and P. V. Kamat, *ACS Energy Lett.*, 2022, **7**, 1994–2011.
17 R. Ketavath, L. Mohan, R. R. Sumukam, Q. A. Alsulami, A. Premalatha and B. Murali, *J. Mater. Chem. A*, 2022, **10**, 12317–12333.
18 X. Zhu, Y. Lin, J. San Martin, Y. Sun, D. Zhu and Y. Yan, *Nat. Commun.*, 2019, **10**, 2843.
19 Q. Fan, L. Zhu, X. Li, H. Ren, H. Zhu, G. Wu and J. Ding, *New J. Chem.*, 2021, **45**, 13317–13322.
20 A. Shi, K. Sun, X. Chen, L. Qu, Y. Zhao and B. Yu, *Org. Lett.*, 2022, **24**, 299–303.
21 Q. Fan, H. Zhang, D. Liu, C. Yan, H. Zhu, Z. Xie and Z. Le, *J. Org. Chem.*, 2023, **88**, 7391–7400.
22 X. Liu, R. Bai, Z. Guo, Y. Che, C. Guo and H. Xing, *Appl. Organomet. Chem.*, 2022, **36**, e6492.
23 L. De Trizio, I. Infante and L. Manna, *Acc. Chem. Res.*, 2023, **56**, 1815–1825.
24 B. Chen, L. Wang and S. Gao, *ACS Catal.*, 2015, **5**, 5851–5876.
25 M.-Y. Qi, M. Conte, Z.-R. Tang and Y.-J. Xu, *ACS Nano*, 2022, **16**, 17444–17453.
26 J.-H. Zheng, M.-Y. Qi, Z.-R. Tang and Y.-J. Xu, *J. Mater. Chem. A*, 2023, **11**, 4013–4019.
27 L. Protesescu, S. Yakunin, M. I. Bodnarchuk, F. Krieg, R. Caputo, C. H. Hendon, R. X. Yang, A. Walsh and M. V. Kovalenko, *Nano Lett.*, 2015, **15**, 3692–3696.
28 Y. Kim, D. Dumett Torres and P. K. Jain, *Nano Lett.*, 2016, **16**, 3399–3407.
29 A. U. Rehman, F. Bashir, F. Ayaydin, Z. Kóta, T. Páli and I. Vass, *Physiol. Plant.*, 2021, **172**, 7–18.
30 S. Swaminathan, V. G. Rao, J. K. Bera and M. Chandra, *Angew. Chem., Int. Ed.*, 2021, **60**, 12532–12538.
31 N. Fiuza-Maneiro, K. Sun, I. López-Fernández, S. Gómez-Graña, P. Müller-Buschbaum and L. Polavarapu, *ACS Energy Lett.*, 2023, **8**, 1152–1191.
32 E. Bordignon, *eMagRes*, John Wiley & Sons, Ltd, 2017, pp. 235–254.
33 N. Serpone and A. V. Emeline, *J. Phys. Chem. Lett.*, 2012, **3**, 673–677.
34 D. B. Ushakov, M. B. Plutschack, K. Gilmore and P. H. Seeberger, *Chem. – Eur. J.*, 2015, **21**, 6528–6534.
35 S. Maity and N. Zheng, *Synlett*, 2012, 1851–1856.
36 J. De Roo, M. Ibáñez, P. Geiregat, G. Nedelcu, W. Walravens, J. Maes, J. C. Martins, I. Van Driessche, M. V. Kovalenko and Z. Hens, *ACS Nano*, 2016, **10**, 2071–2081.
37 Z. Hens and J. C. Martins, *Chem. Mater.*, 2013, **25**, 1211–1221.

